TOWARDS BATTERY-FREE WIDE AREA NETWORK WITH ULTRA-LOW VOLTAGE CHIRP SPREAD SPECTRUM MODULATION

Anthony Bres
Univ. Bordeaux, CNRS, Bordeaux INP,
IMS, UMR 5218,
F-33400 Talence, France
Anthony.bres@enseirb-matmeca.fr

Valentin Guillerat
Univ. Bordeaux, CNRS, Bordeaux INP,
IMS, UMR 5218,
F-33400 Talence, France
valentin.guillerat@enseirb-matmeca.fr

Guillaume Ferré
Univ. Bordeaux, CNRS, Bordeaux INP,
IMS, UMR 5218,
F-33400 Talence, France
g uillaume.ferre@ims-bordeaux.fr

Simon Hemour
Univ. Bordeaux, CNRS, Bordeaux INP,
IMS, UMR 5218,
F-33400 Talence, France
simon.hemour@ims-bordeaux.fr

***Abstract*— Next generation of wireless sensors networks is poised to operate at zero-power. To reach this goal while operating over long range, there is a need for ultra-efficient RF transmitter and associated modulation techniques. The spread spectrum modulation for digital communication features best in class advantages, with its robustness to narrow band interference or its ability of the receiver and demodulate signals with extra low SNR. The objective of this paper is to propose a charge-to-chirp circuit capable of producing this modulation. Unlike competing architectures, this ultra-low voltage transmitter is capable of generating a spread waveform of the CSS type. It implements a tunnel-diode–based voltage-controlled-oscillator driven by ramp generator cells. Chirp of spreading factors SF=6 are demonstrated with the circuit. The VCO is driven by 300 mV capacitor micro-discharges (power consumption of 280 µW) and produces has an output power of - 12dBm. This characteristic allows to consider the deployment of a long range wide area network transmitter operating without battery.**

Keywords—Chirp spread spectrum, Tunnel diode, extra low power, batteryless, LoRa.

I. INTRODUCTION

There is a need to push technology towards long term, sustainable goals rather than letting it being pulled by short-term market objectives. For example, many methods of production of our societies are not fitted for low energy consumption or low equivalent CO2 emission [1], leading to an inexorable scarcity of resources.

Fortunately, those processes are today well identified, and can be easily improved with more feedback. That's where energy-autonomous wireless sensors come into play. For instance in precision agriculture, sensors will provide field knowledge of crop state, so that over-applying or under-applying nutrient and water can be avoided [2]. In buildings heating systems, temperature sensor and occupancy sensors can help avoiding over-heating and over-wasting fuel or electricity [3] The urge for greener technologies puts then massive stress on wireless sensors research to improve its energy autonomy in the context of appropriate communication ranges. As a matter of fact, energy autonomy can be enhanced by the concurrent use of (i) extra low power functions, and (ii) micro-energy generators.

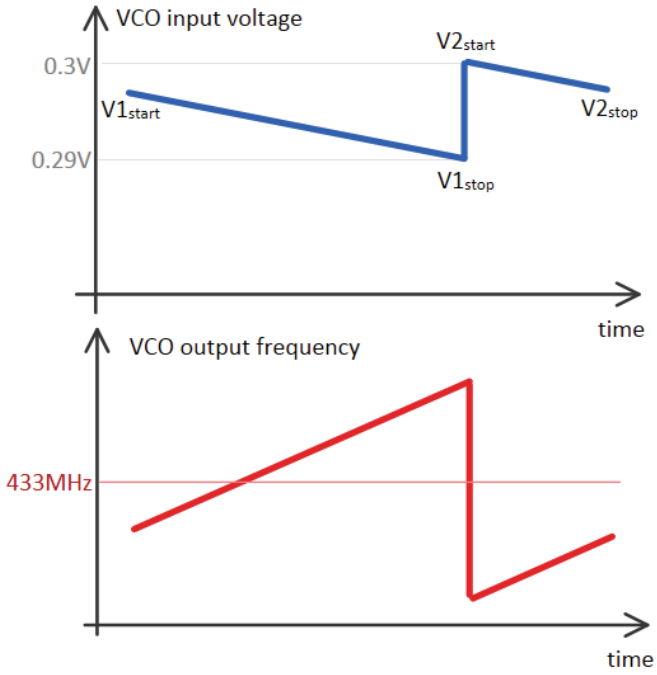

Fig. 1. Chirp spread spectrum (CSS) modulation reported in this paper is generated using a tunnel diode voltage controlled oscillator (VCO) operating under ultra-low voltage. The frequency chirps (red) are a direct conversion of pseudo-linear voltage ramps (blue), which are created by capacitor discharges.

To make the best use of limited power ressources, highly power-efficient wireless communication scheme need to be implemented. This is typically the case of Chirp Spread Spectrum (CSS) modulation, which can fight with noise on the receiver side down to below -140dBm, such as it is the case for Long Range (LoRa) patented technology [4-6]. Thanks to the possible adjustment of its modulation parameters, such as the bandwidth, the coding rate, and the spreading factor the CSS modulation already addresses a multitudes of applications. Very interestingly, many communication can be supported on the same frequency and same channel when using different spreading factor, since they are orthogonal.

Using "micro-sources" is a critical way for reaching batteryless sensors. Those systems have the endless capability

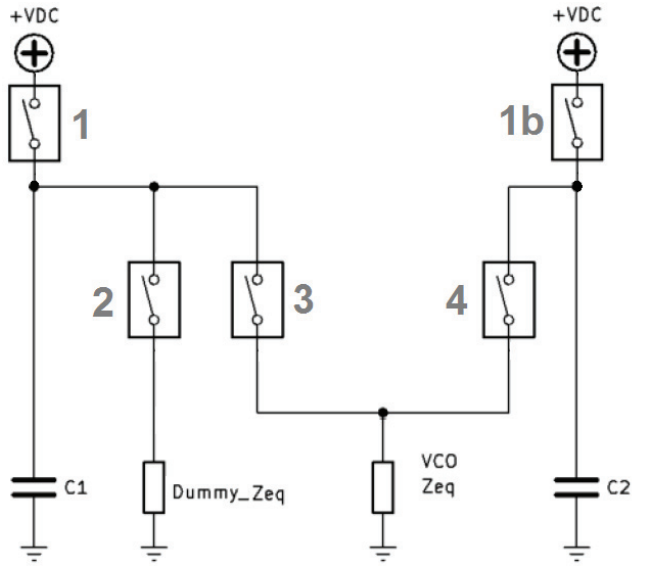

Fig. 2 Diagram of the baseband CSS ramp generator cell. The principle of operation follows: All switches are *normally OFF*. During the setting phase switches 1 and 1b are closed to charge C1 and C2 to voltage V_0. Then, before engaging the chirp generation, the switch 2 is used to discharge the capacitance C1 to reach the voltage $V1_{start}$ (as described in the Fig. 1). When the first segment of the chirp needs to be fired, the switch 3 is used to discharge capacitor C2 into the VCO until voltage $V1_{stop}$ is reached. Then switch 4 is used to discharge C2 into the VCO to produce the second segment of the chirp. (see switching chronology in time domain in figure 8)

to harvest ambient, ubiquitous, spatially distributed energy that is by definition renewable, such as: solar radiation [7], even kinetic energy [8-9] and ambient RF wireless telecommunication signal energy [10-12]. Unfortunately, the regular operation of those energy harvester, at which the maximum energy conversion efficiency is achieved yields too low output voltage [13] for the industry standards (radio frequency LoRa chips typically require 3V to operate). Because of this, inefficient strategies are commonly implemented such as: voltage booster, voltage multiplier, and lining up of multiple harvesters [15]. This leads to significant downfall of the wireless sensor power efficiency.

This paper introduces an ultra-low voltage CSS modulator with voltage operation down to 0.3V. It is based on charges-to-chirp conversion circuit, where every chirp section is generated by a capacitor discharge. This circuit includes a ramp generator and a tunnel diode-based voltage controlled oscillator. The next sections describes the operation principle of the ramp generator and the design details on the tunnel diode VCO. Finally, the paper then reports measurement of generated CSS signals.

II. Basic principle

A classical CSS communication is composed of a set of two raw chirps which are delayed to encode data. A symbol can then be seen as a juxtaposition of two chirp sections with a transition at the delay value (fig. 1). The proposed strategy is to build a circuit capable of driving the VCO with two analogue ramps to synthesise any possible CSS symbols. The diagram of the ramp generator is provided in figure 2. With the architecture, various ramps can be created. To provide a single time constant (and therefore controlled ramp slope) throughout the circuit, C1 and C2 need to be set to equal values. It is also the case for the VCO equivalent DC resistance and its relative dummy load. Thanks to this feature, the operation of the ramp generator remain identical,

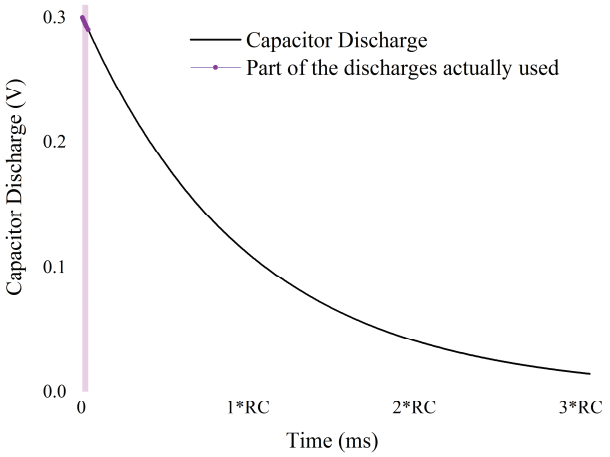

Fig.3. Capacitance discharge during a duration << time constant is used to provide a pseudo linear voltage ramp to drive the VCO (bold, purple part of the curve)

irrespective to the switch configuration, and the circuit's switches can be controlled though time delays rather than by monitoring the resulting output voltage.

Generating linear chirp is an important factor for enabling the dynamic range of CSS receiver. Toward this end, the ramp generator is set to use only 4% of the complete capacitor discharge capabilities, starting from 0.3V to 0.29V (Figure 3), to guaranty minimum nonlinearity of the pseudo linear ramp.

Since the equivalent DC resistance of the VCO is fixed, the capacitor value of C1 and C2 can be chosen to match with desired chirp shape as well as the bandwidth for a given Ts symbol time discharge. The time constant of the capacitor discharging into the VCO is given by :

$$\tau = R_{eq}C \text{, with } R_{eq} = \frac{< U_C >}{< I_C >} \quad (1)$$

Given the slope of the frequency response of the VCO in next section, and given the typical bandwidth of a 433MHz chirp B = 125kHz this implies that the capacitor must be discharged by only about ten mV during the duration of the Ts symbol. To generate a pseudo linear ramp, we choose t >> Ts, and therefore approximate the discharge of the capacitor as linear for the estimation of the equivalent resistance of the VCO. Thus for a discharge starting at $U_C = U_{C\_max}$ and ending at $U_C = U_{C\_min}$ after t = Ts seconds we have

$$< U_C >= U_{Cmin} + \frac{\Delta_{U_C}}{2} \text{ and } < I_C >= I_{Cmin} + \frac{\Delta_{I_C}}{2} \quad (2)$$

During the discharge, we are facing a classical RC circuit, so we have as equation of the voltage across the capacitor voltage across the capacitor :

$$U_C(t) = U_{Cmax} e^{-\frac{t}{R_{eq}C}} \quad (3)$$

Placing ourselves at the instant Ts we have $U_C(t) = U_{Cmin}$, with which one can calculate the required capacitance for the operation:

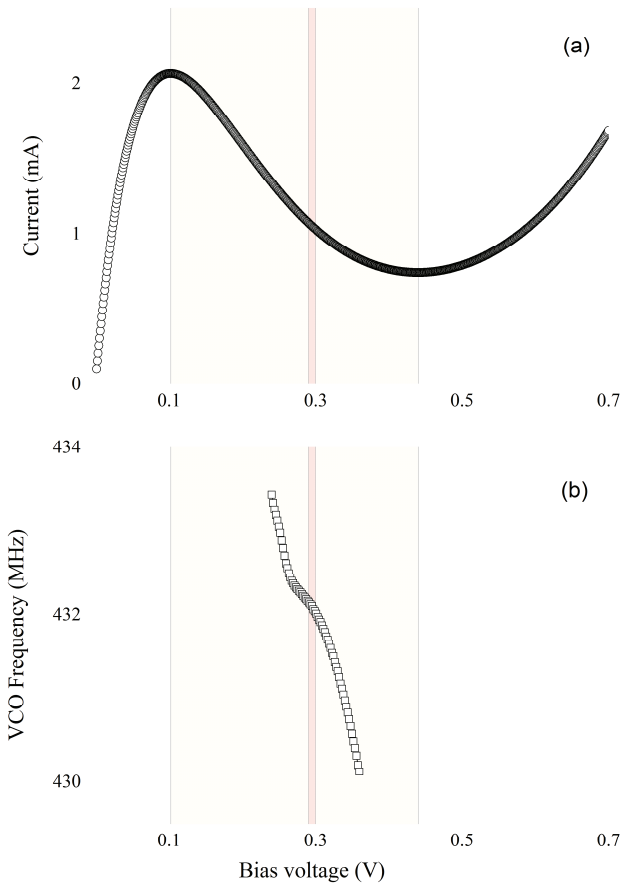

Fig.4. (a) Current-Voltage characteristic of the tunnel diode used in this work. The red area corresponds to the operation range in this work. As the capacitance is discharging in to the tunnel diode VCO over time, it passes through all the current-voltage characteristics of the tunnel diode, corresponding to different oscillation frequencies, resulting in the creation of a chirp; (b) Frequency response of the Tunnel diode VCO

$$C = \frac{-T_s}{ln(\frac{U_{Cmin}}{U_{Cmax}})R_{eq}} \quad (4)$$

Aside from the switches, there are no other active devices used with this strategy to drive the VCO. The charge-to-chirp operation described here is therefore seen as an energy-efficient process

III. VCO

The measured current-voltage characteristic of the 3И306E tunnel diode is shown in Figure 4-a. Between 0.1 V and 0.42 V, the current decreases as the bias voltage increases. This corresponds to an inherent dynamic negative resistance which is perfectly suited for free running oscillator operation. Since the junction capacitance and inherent dynamic negative resistance of the tunnel diode are both sensitive to bias voltage [15, 16], this device is especially appropriate for frequency modulation. It is not shown here, but as the bias voltage is risen, those two parameters monotonically increase, leadind to a reduction of the oscillating frequency.

As seen in fig. 4-b, the resulting oscillating frequency is indeed decreasing as a function of input voltage bias. Note that the tuning characteristics of the VCO exhibit non-linearites. This can be very useful to choose the tuning range of the circuit. Because the ISM bands requires narrowband use, a low sensitivity is desirable (meaning narrow frequency

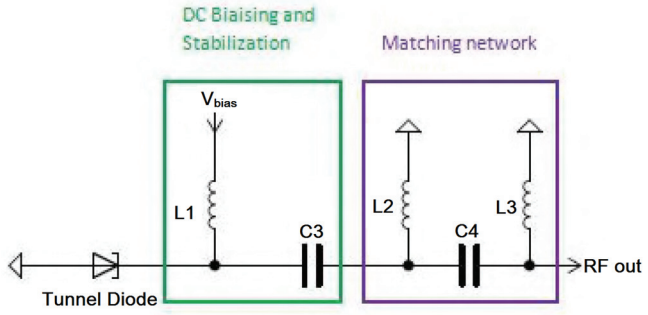

Fig.5. Schematic of the 433MHz tunnel diode voltage controlled oscillator

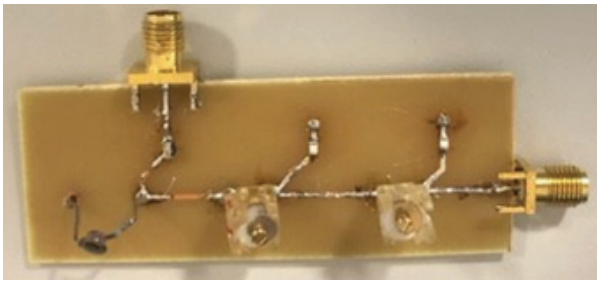

Fig.6. Photograph of the 433MHz tunnel diode voltage controlled oscillator

range for a given range of tuning voltage). For this reason, the plateau of the V/f slope is chosen (fig. 4-b), and operation condition is set to be maximum 300mV (highest ramp voltage). This value is of high importance in our system because it corresponds eventually to the ramp generator capacitor charging voltage.

The VCO circuit is given in figure 5 and 6, with component value described in table 1.

Component value for the VCO circuit		
subcircuit	***Part***	***Value***
DC Biasing & Stabilisation	L1	22nH
	C3’	4pF
Matching network	L2, L3	10n H
	C4’	4pF
tunnel Diode	3И306E	Ip=2mA

IV. MEASUREMENT RESULTS

To validate the ultra-low voltage chirp spread spectrum modulator, the VCO is driven by the ramp generator, which switches are controlled by an ATMEGA328P microcontroller. The latter is not meant to be part of the system, but has been helpful for demonstrating the proof of principle.

The operation of one ramp generator cell (as shown in Fig.2) is demonstrated in fig. 7, while three different cells are being implemented and used circularly for the real case shown in fig. 8. Thanks to this circular operation, at any given time of the transmission:

- one cell is in use to drive the VCO for the symbol generation, while
- the second cell is readying the C1 voltage value for the next symbol, while
- The third cell is charging C1 and C2.

In the experiments performed here, the charging time of the capacitors were lesser than a symbol time. In real condition

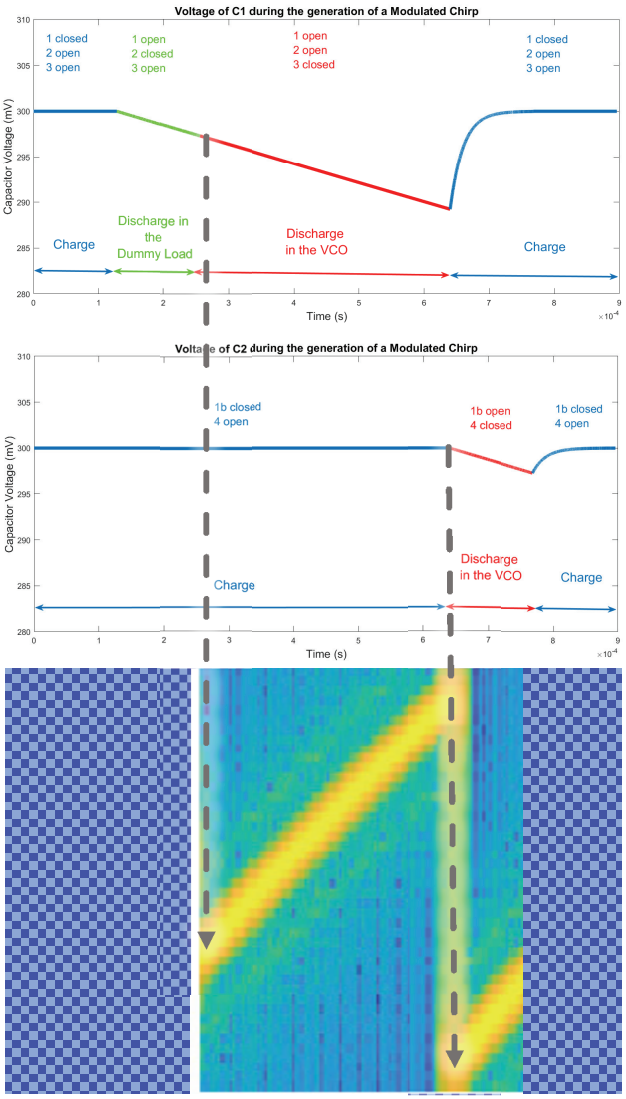

Fig. 7. The two chirp sections are fired successively to build a symbol. (a) Voltage of C1 during the generation of the first section of the symbol; (b) Voltage of C2 during the generation of the second section of the symbol (c) resulting symbol as generated by the VCO (Example for a 0b10 binary value coded on 4 symbols, corresponding to a delayed chirp of $= \frac{3\,T_s}{4}$)

with larger charging time, more cells can be considered. Particularly, for batteryless IoT field operation a set of given cells can be implemented, with concordance to the number of symbols to be transmitted. In such scenario, transmission would not start until all would be ready.

The switch implemented in the ramp generator cells to manage the discharge is the N-inputs/single output TMUX1108PWR (either directing current into the VCO or in the dummy load). To charge multiple capacitors at the same time the single input/N-output ADG711BRZ switch is in turn implemented.

To demonstrate the capability of the prototype to generate a frame, a CSS waveform as depicted in fig. 8, for a spreading factor of SF≈6. In this example, the 4 different symbols are transmitted based on the following binary sets: 00, 01, 10, 11.

V. Conclusion

This modulation strategy is very simple and could be easy to deploy. Its VCO It uses 300mV and 280µWf. However, such technique might need advanced calibration techniques to

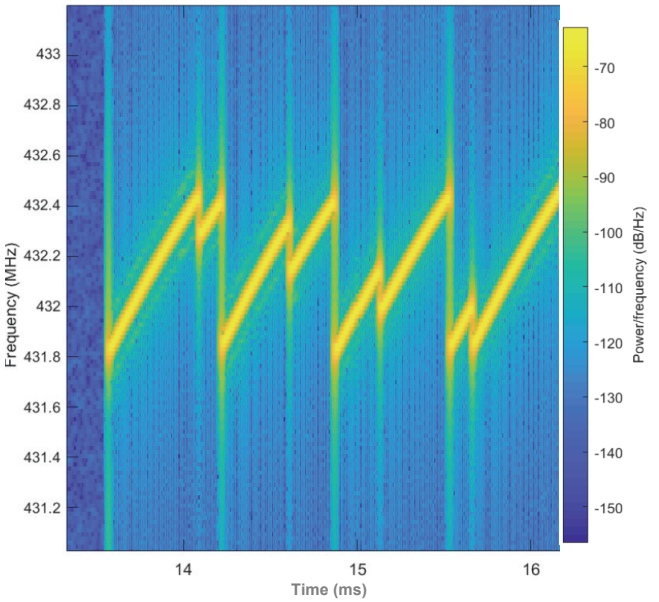

Fig. 8 Spectrogram of the 4 symbols generated with the modulator circuit (00, 01, 10 11)

account for the chirp nonlinearity and the variation tolerance value in the ramp generator. This will be developed in a further work. The charge to chirp principle is seen as radically different from that of conventional modern digitak modulator that are all using based on PLL and quartz oscillator. Other improvement include the engineering of the chirp slope to improve the linearity of the chrirps symbols. Lastly, Ihe circuit is meant to be used as a power VCO, meaning no power amplifier to be used. Therefore pulling antenna effects on the circuit need to be further investigated

References

[1] W. E. REES, and M. WACKERNAGEL, The shoe fits, but the footprint is larger than earth. *PLoS biology,* 2013, vol. 11, no 11, p. e1001701.

[2] R. BONGIOVANNI, and J. LOWENBERG-DEBOER. Precision agriculture and sustainability. *Precision agriculture,* 2004, vol. 5, no 4, p. 359-387.

[3] B. DONG, and K. P. LAM, A real-time model predictive control for building heating and cooling systems based on the occupancy behavior pattern detection and local weather forecasting. *In : Building Simulation. Springer Berlin Heidelberg*, 2014. p. 89-106.

[4] https://www.semtech.com/products/wireless-rf/lora-core/sx1302

[5] L-T TU, A. BRADAI, Y. POUSSET, et al. Energy Efficiency Analysis of LoRa Networks. *IEEE wireless communications letters*, 2021, vol. 10, no 9, p. 1881-1885.

[6] D BELO, R CORREIA, et al, IQ impedance modulator front-end for low-power LoRa backscattering devices, *IEEE Transactions on Microwave Theory and Techniques* 67 (12), 5307-5314, 2019

[7] M. GREEN, Thin-film solar cells: review of materials, technologies and commercial status, *Journal of Materials Science: Materials in Electronics,* vol. 18, no. 1, pp. 15-19, 2007/10/01 2007.

[8] X GU, S HEMOUR, et al., Integrated cooperative ambient power harvester collecting ubiquitous radio frequency and kinetic energy, *IEEE Transactions on Microwave Theory and Techniques* 66 (9), 4178-4190, 2018

[9] X GU, L GUO, et al., Optimum temperatures for enhanced power conversion efficiency (PCE) of zero-bias diode-based rectifiers, *IEEE Transactions on Microwave Theory and Techniques* 68 (9), 4040-4053, 2020

[10] E VANDELLE, TP VUONG, et al., Harvesting ambient RF energy efficiently with optimal angular coverage *IEEE Transactions on Antennas and Propagation* 67 (3), 1862-1873, 2019

[11] L GUO, X GU, et al., Collaboratively harvesting ambient radiofrequency and thermal energy, *IEEE Transactions on Industrial Electronics* 67 (5), 3736-3746, 2019

[12] X GU, L GRAUWIN, et al., Dynamic ambient RF energy density measurements of Montreal for battery-free IoT sensor network planning, *IEEE Internet of Things Journal* 8 (17), 13209-13221, 2021

[13] X GU, P BURASA, Recycling ambient RF energy: Far-field wireless power transfer and harmonic backscattering *IEEE Microwave Magazine* 22 (9), 60-78, 2021

[14] M PIÑUELA, PD MITCHESON, S LUCYSZYN, Ambient RF energy harvesting in urban and semi-urban environments, *IEEE Transactions on microwave theory and techniques* 61 (7), 2715-2726, 2013

[15] F AMATO, S HEMOUR, The harmonic tunneling tag: A dual-band approach to backscattering communications, *2019 IEEE International Conference on RFID Technology and Applications (RFID-TA), 2019*

[16] K GUMBER, C DEJOUS, et al., Harmonic reflection amplifier for widespread backscatter Internet-of-Things, *IEEE Transactions on Microwave Theory and Techniques* 69 (1), 774-785, 2020